AGU PUBLICATIONS

Geophysical Research Letters

RESEARCH LETTER
10.1002/2015GL067241

Key Points:
- Diurnal variation of the Fe layer bottomside now explained
- Combination of approaches to determine an important photolysis rate for the first time
- Implications for the Fe speciation in meteoric smoke particles

Correspondence to:
T. P. Viehl,
viehl@iap-kborn.de

Citation:
Viehl, T. P., J. M. C. Plane, W. Feng, and J. Höffner (2016), The photolysis of FeOH and its effect on the bottomside of the mesospheric Fe layer, *Geophys. Res. Lett.*, *43*, 1373–1381, doi:10.1002/2015GL067241.

Received 14 DEC 2015
Accepted 21 JAN 2016
Accepted article online 28 JAN 2016
Published online 11 FEB 2016

The photolysis of FeOH and its effect on the bottomside of the mesospheric Fe layer

T. P. Viehl[1], J. M. C. Plane[2], W. Feng[2,3], and J. Höffner[1]

[1] Leibniz-Institute of Atmospheric Physics, University of Rostock, Kühlungsborn, Germany, [2] School of Chemistry, University of Leeds, Leeds, UK, [3] National Centre for Atmospheric Science, School of Earth and Environment, University of Leeds, Leeds, UK

Abstract Metal layers in the upper mesosphere and lower thermosphere are created through meteoric ablation. They are important for understanding the temperature structure, dynamics, and chemistry of this atmospheric region. Recent lidar observations have shown a regular downward extension of the Fe layer bottomside which correlates with solar radiation. In this study we combine lidar observations, quantum chemical calculations, and model simulations to show that this bottomside extension is primarily caused by photolysis of FeOH. We determine the photolysis rate to be $J(\mathrm{FeOH}) = (6 \pm 3) \times 10^{-3}$ s^{-1}. We also show that the reaction FeOH + H → FeO + H_2 is slower at mesospheric temperatures than previous estimates. With these updated rate coefficients, we are able to significantly improve the modeling of the Fe layer bottomside. The calculations further show the nearly complete depletion of FeOH during sunlit periods. This may have implications for cloud nuclei in the middle atmosphere.

1. Introduction

Layers of metal atoms are created in the region of the upper mesosphere and lower thermosphere (MLT, ~70–110 km) through meteoric ablation. These layers are important for understanding the temperature structure dynamics and chemistry of this atmospheric region [e.g., *Lübken et al.*, 2015; *Feng et al.*, 2015; *Yu et al.*, 2012], the influx of cosmic material [e.g., *Plane*, 2012; *Gardner et al.*, 2014; *Huang et al.*, 2015], and the occurrence of thermospheric and sporadic metal layers and their relation to sporadic *E* layers which can influence radio wave propagation [e.g., *Chu et al.*, 2011; *Delgado et al.*, 2012]. Furthermore, meteoric metals are the source of meteoric smoke particles (MSPs) which most likely act as nuclei for ice particles in the mesosphere [e.g., *Gumbel and Megner*, 2009; *Megner and Gumbel*, 2009] and may also interact with sulphuric and nitric acid in the stratosphere [*Saunders et al.*, 2012; *Frankland et al.*, 2015]. A recent review on the chemistry of metals in the MLT region summarizes the current understanding and highlights open questions [*Plane et al.*, 2015]. It shows the importance of understanding all chemical reactions, the metals and their molecular species undergo, so that atmospheric chemistry models can correctly describe the dynamical behavior of the metal layers to give insights into some of the topics mentioned above. Laboratory studies have provided a broad insight into many of the important reactions dominating the MLT metal layers. However, some important chemical reactions with metal-containing species do not have a suitable electronic transition for probing by laser-induced fluorescence and could so far not be investigated directly.

The atomic Fe layer at polar latitudes has a mean centroid altitude of around 88 km. Recent lidar observations at polar latitudes show a downward extension of the layer below 80 km during sunlit periods [*Yu et al.*, 2012]. *Self and Plane* [2003] and *Plane* [2003] have shown that FeOH should be the dominant reservoir for atomic Fe below 95 km. As *Plane et al.* [1999] have illustrated, one way to dissociate FeOH at sunrise is via reaction with atomic H which is produced by photolysis of H_2O in sunlit periods. However, during nighttime the concentration of this radical decreases rapidly below ~82 km, so that FeOH becomes a stable reservoir for Fe. Within the current understanding, atmospheric chemistry models such as Whole Atmosphere Chemistry Climate Model (WACCM)-Fe [*Feng et al.*, 2013] have so far been unable to correctly reproduce the bottomside extension of the Fe layer. Here we present a study combining atmospheric lidar observations, quantum chemical calculations, and atmospheric modeling to derive the photolysis rate of FeOH, *J* (FeOH), which so far has not been measured. We show that only the direct photolysis of FeOH can be fast enough to explain the bottomside

extension of the mesospheric Fe layer at sunrise. The combination of methods described here also allows us to place upper limits to the rate coefficients under mesospheric conditions for the reactions

$$FeOH + H \rightarrow Fe + H_2O \quad (1a)$$

$$\rightarrow FeO + H_2 \quad (1b)$$

2. Atmospheric Observations

2.1. Instrument and Data Set

The Leibniz-Institute of Atmospheric Physics operates a mobile Fe lidar based on a frequency-doubled alexandrite laser scanning the Doppler broadened Fe resonance line at 386 nm [*von Zahn and Höffner*, 1996; *Höffner and Lautenbach*, 2009]. The system is capable of nearly background free single photon detection and can determine mesospheric Fe densities in full daylight. Typical measurement uncertainties are on the order of 2–5% at 1 km resolution and 15 min integration.

The Fe lidar was set up at Davis, Antarctica (68°34′S, 77°58′E), in 2010 and was in operation from 15 December 2010 until 31 December 2012 [e.g., *Lübken et al.*, 2011; *Viehl et al.*, 2015; *Lübken et al.*, 2015]. The data set obtained in Antarctica includes 2900 h of Fe density measurements. In the years 2008–2009 and since July 2014, the system has been in operation at the Arctic Lidar Observatory for Middle Atmosphere Research (ALOMAR) on the Norwegian Island of Andøya (69°16′N, 16°00′E). The observations in the Arctic have so far produced more than 1200 h of Fe density measurements.

2.2. Observation and Analysis of the Fe Layer Bottomside

Figure 1 shows two examples of mesospheric Fe layer observations in the summer of the Southern Hemisphere and the winter of the Northern Hemisphere. The pronounced change in the Fe layer below 80–85 km is regularly observed in both hemispheres and all seasons whenever the solar elevation passes a critical level around −5°; i.e., the MLT experiences sunrise or sunset. *Yu et al.* [2012] investigated the diurnal behavior of the mesospheric Fe layer at McMurdo, Antarctica (78°), and defined the "bottomside" as the lower 300 cm^{-3} contour. That study analyzed the time-dependent altitude change $\frac{\Delta z}{\Delta t}$ of the defined contour and found a dependence on the time of the season, caused by the change of solar elevation.

In this study, we analyze the rate of change of Fe density, $\frac{\Delta[Fe]}{\Delta t}$, over an altitude interval of 1 km, thereby quantifying the rate of increase of Fe at each altitude's time of apparent sunrise. The rate of increase is described by direct photolysis ($FeOH + h\nu$) and chemical reactions (1a) and (1b) producing Fe. We note that although reaction channel (1b) produces FeO, this will mostly be reduced to Fe by subsequent reaction of FeO with atomic O in the sunlit MLT. Further reactions cannot contribute significantly, as other reservoirs are less abundant by 2–4 orders of magnitude [*Feng et al.*, 2013] and additional reaction pathways from FeOH to Fe are not known. As a first approximation, the time-dependent Fe concentration $[Fe]_t$ produced by photolysis of FeOH is given by

$$[Fe]_t = [FeOH]_0 \, (1 - \exp(-Jt)) \quad (2)$$

where $J = J(FeOH)$ is the photolysis rate of FeOH and $[FeOH]_0$ is the concentration just before sunrise. Since the resulting Fe will be oxidized via a sequence of reactions involving O_3, O_2, and H_2O to reform FeOH [*Plane et al.*, 2015], the observed rate of increase of Fe at sunrise provides a lower limit to J(FeOH).

Figure 2 shows an example of a single day where we have analyzed the rate of increase at sunrise. Figure 2a shows the bottomside extension between 5 and 9 local solar time (LST). The main Fe layer with densities higher than 6000 cm^{-3} is observed above about 82 km. The bottomside extension of the Fe layer builds up below 80 km from 7 LST, extending down to 70 km by 8 LST. The cutoff for Fe densities in Figure 2a is 100 cm^{-3}. Figure 2b shows the analysis of a single altitude. Densities at 76 km are below the cutoff during the night and quickly increase at sunrise. The time to reach $[Fe]_{t1/2} = 0.5 \times [Fe]_{tmax}$ can be used to determine a lower limit for J(FeOH) when setting $[FeOH]_0 = [Fe]_{tmax}$ in equation (2), assuming a full conversion of FeOH to Fe.

We have analyzed all available cases of the bottomside extension at various altitudes for both hemispheres (Davis, 69°S and ALOMAR, 69°N). We averaged the photolysis coefficients determined using equation (2) for

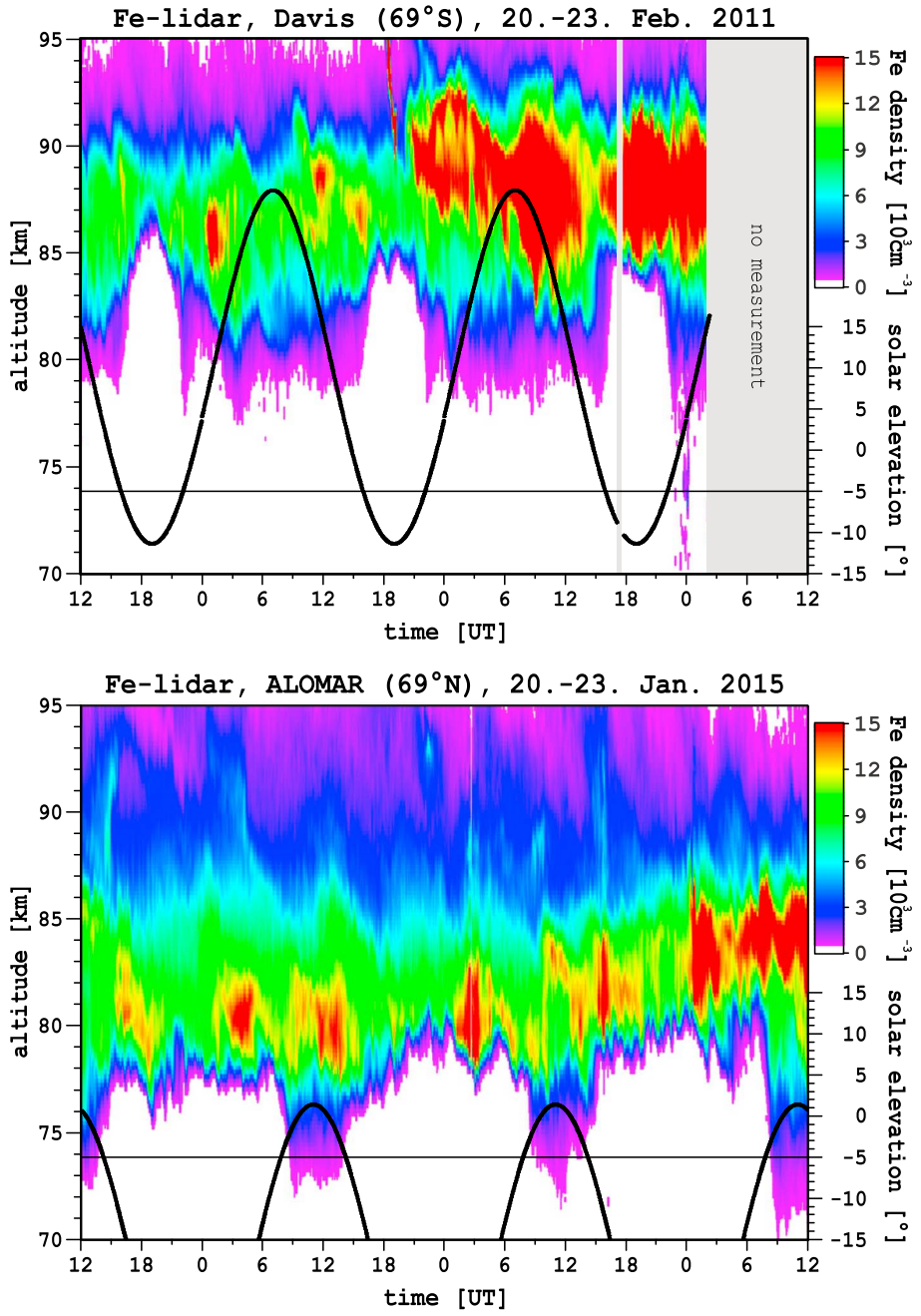

Figure 1. The mesospheric Fe layer at (top) Davis, Antarctica (69°S), and (bottom) ALOMAR, Norway (69°N) during three consecutive cycles of sunset and sunrise. An extension of the metal layer's bottomside is observed whenever sunlight reaches the MLT region.

all days and altitudes to remove the distortions caused by gravity waves (which are observable in Figure 1). The difference between the hemispheres is much smaller than the variability given as the standard deviation. The combined average first-order coefficient observed by lidar is $(1.2 \pm 0.4) \times 10^{-3}$ s^{-1}. We will show that this corresponds to a photolysis coefficient, setting a lower limit to J (FeOH).

3. Theoretical Considerations

To separate the influence of the photolysis and the reactions of FeOH with H and to compare with the observed rate of increase, we have performed quantum chemical calculations and revisited previous laboratory studies.

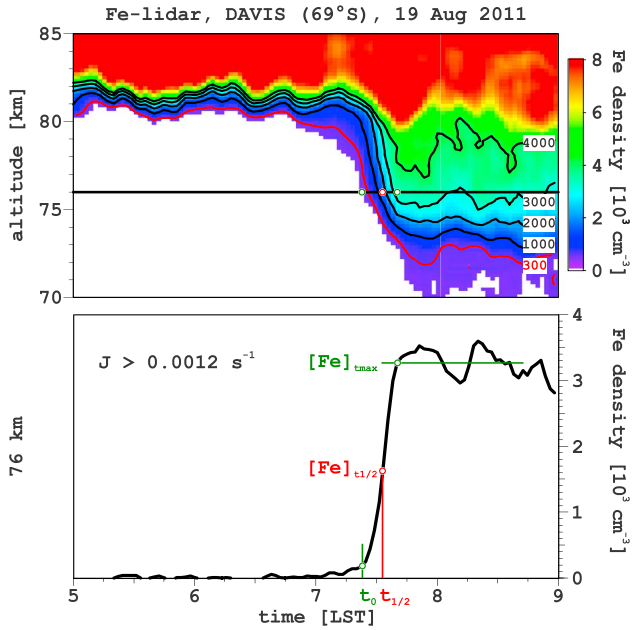

Figure 2. The rate of increase of Fe at sunrise is analyzed at different altitudes for all available days of lidar observations in the Arctic and Antarctica. Analysis of all available days yields a mean rate of $(1.2 \pm 0.4) \times 10^{-3}$ s^{-1}, which is a lower limit to J(FeOH) because of recycling of Fe to FeOH (see text). Of the available reactions, only the direct photolysis of FeOH can be fast enough to explain such a rapid increase.

3.1. Photolysis of FeOH

To calculate the absorption cross section of FeOH, the molecular geometry was first optimized using the range-separated CAM-B3LYP functional [*Yanai et al.*, 2004] and the 6-311+g(2d,p) basis set in the Gaussian 09 suite of programs [*Frisch et al.*, 2009]. The equilibrium structure of the ground state (X^6A') is bent with r_e(Fe–O) = 1.793 Å, r_e(O–H) = 0.957 Å, and $\angle_e$(Fe–O–H)=142.0°. The energies and transition oscillator strengths for vertical transitions to the first 30 excited states were then computed using the time-dependent (TD) density functional method [*Scalmani et al.*, 2006]. The long-range correction in the TD/CAM-B3LYP functional makes it suitable for modeling electron excitations to high-lying orbitals.

Figure 3 illustrates the calculated photolysis cross section as a function of wavelength ($\sigma(\lambda)$) for FeOH. The bond energy of FeOH at 0 K is 323 ±16 kJ mol^{-1} [*Schröder*, 2008], which corresponds to a thermodynamic

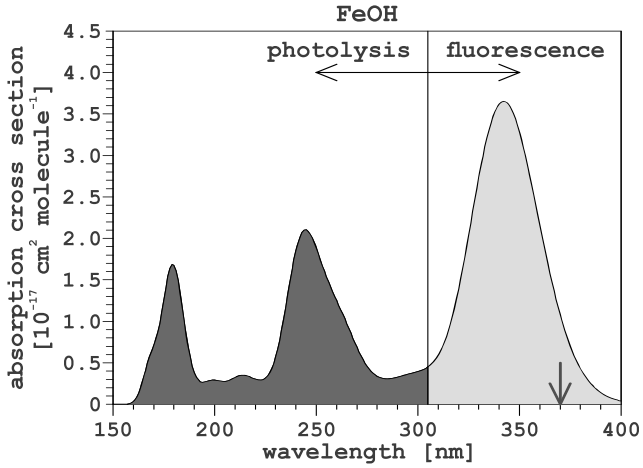

Figure 3. Absorption cross section for FeOH calculated at the TD/CAM-B3LYP/6-311+g(sd,p) level of theory. Wavelengths shorter than ~305 nm lead to photolysis.

threshold for photolysis of 370 nm (vertical arrow in Figure 3). However, absorption in the large band between 300 and 400 nm does most likely not lead to photolysis. Two pieces of evidence support this.

First, FeOH is electronically analogous to FeCl. Our calculations show that FeCl has a very similar absorption spectrum to FeOH, and absorption between 315 and 370 nm produces fluorescence in FeCl rather than dissociation [*Delaval et al.*, 1980; *Lei and Dagdigian*, 2000]. Second, inspection of the Mulliken electron populations of the excited states of FeOH shows that these remain ionic like the ground state up to the seventh state. Only the eighth and higher states are covalent and hence more likely to dissociate to Fe + OH. The transition to the eighth state is calculated to occur at 300 nm, so the threshold for photolysis should be slightly red shifted (allowing for internal excitation).

The photolysis coefficient is then computed from the relation

$$J = \int_{\lambda_1}^{\lambda_2} \sigma(\lambda)\Phi(\lambda)\mathrm{d}\lambda$$

where $\Phi(\lambda)$ is the solar actinic flux by the semiempirical model SOLAR2000 averaged over a solar cycle [*Tobiska et al.*, 2000]. The integration is performed from 305 to 150 nm, yielding $J(\mathrm{FeOH}) = 6.2 \times 10^{-3}$ s^{-1}. The slight uncertainty in the exact transition from fluorescence to photolysis results in an uncertainty of the photolysis rate of about 50%. The order of magnitude of the photolysis, however, is not affected by this. Note that this value of J (FeOH) is about 5 times larger than the lower limit determined from the analysis of lidar observations in section 2.2. As we show in section 4, this value of J (FeOH) $= (3 - 9) \times 10^{-3}$ s^{-1} compares well with the rate required to match the observed increase of Fe below 80 km.

3.2. Reaction of FeOH With H

The reaction between FeOH and H can proceed via the exothermic channels of reactions (1a) and (1b), where $\Delta H°(0\mathrm{K}) = -171 \pm 16$ and -92 ± 21 kJ mol^{-1}, respectively [*Schröder*, 2008]. Note that H can also react with FeOH to form HFeOH, but this is not important under mesospheric conditions [*Self and Plane*, 2003]. The rate constants for reactions (1a) and (1b) have been determined in studies of Fe-seeded flames at temperatures in excess of 2000 K, indicating that reaction (1b) is the dominant channel even though it is less exothermic [*Jensen and Jones*, 1974; *Rumminger et al.*, 1999]. However, in a subsequent experimental and theoretical study of the FeOH + H reaction, *Self and Plane* [2003] showed that there are significant uncertainties regarding both the relative and absolute rate coefficients for these reactions when extrapolated to around 300 K. Theory indicated that reaction (1a) might be the dominant channel, and so *Feng et al.* [2013] adopted a value of $k_{1a} = 3 \times 10^{-10} \exp(-1264/T)$ cm^3 molecule^{-1} s^{-1} and ignored (1b) for atmospheric modeling purposes. We now reexamine this assumption.

When modeling the underside of the mesospheric Fe layer, a further test of this chemistry is the observed disappearance of Fe between 70 and 80 km at night. Although the atomic H concentration at 70–80 km decreases substantially at night [*Plane et al.*, 2015], sufficient H remains to place upper limits on reactions (1a) and (1b). The rate constant for reaction (1a) from the flame work $k_{1a} = 2 \times 10^{-12} \exp(-600/T)$ cm^3 molecule^{-1} s^{-1} is slow enough at mesospheric temperatures. However, $k_{1b} = 5 \times 10^{-11} \exp(-800/T)$ cm^3 molecule^{-1} s^{-1} [*Jensen and Jones*, 1974] is too fast by around a factor of 5 when extrapolated to 200 K, where k_{1b} needs to be less than 2×10^{-13} cm^3 molecule^{-1} s^{-1}. In order to reproduce the nighttime disappearance of Fe below 80 km in the model, the activation energy and preexponential factor can be increased slightly to $k_{1b} = 6 \times 10^{-11} \exp(-1200/T)$ cm^3 molecule^{-1} s^{-1}, which still gives the rate constant at 2400 K required for flame modeling. These changes are modest bearing in mind the enormous temperature range being extrapolated over.

At typical MLT temperatures of less than 230 K and [H] $\sim 1 \times 10^8$ cm^{-3}, the rates of reactions (1a) and (1b) are on the order of k_{1a} [H] $\sim 1.5 \times 10^{-5}$ s^{-1} and k_{1b} [H] $\sim 3 \times 10^{-5}$ s^{-1}, respectively. Comparison with the value of J (FeOH) determined in section 2.2 shows that these pathways cannot compete with the direct photolysis of FeOH to explain the rate of increase at sunrise. However, at night reactions (1a) and (1b) are probably of similar significance in defining the Fe layer bottomside.

4. Atmospheric Modeling

A series of models for MLT metal chemistry has recently been developed on the basis of the Whole Atmosphere Community Climate Model (WACCM) [*Marsh et al.*, 2013a, 2013b; *Feng et al.*, 2013; *Plane et al.*, 2014;

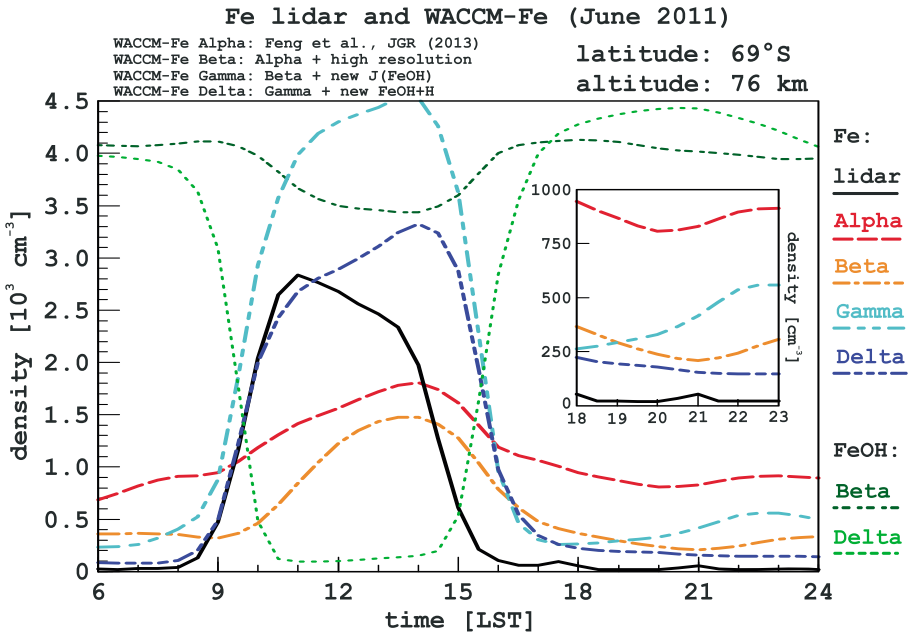

Figure 4. Comparison of the bottomside extension of the Fe layer at Davis, Antarctica, measured by resonance lidar and simulated with WACCM-Fe. Included are four model runs for Fe and two runs for FeOH. The previously existing model run (Alpha) underestimated the increase of Fe observed by lidar at sunrise but overestimated densities during dark periods. New model simulations with higher resolution as well as new rate coefficients for the photolysis of FeOH and the reactions of FeOH capture the observed behavior, in particular the crucial rate of increase at sunrise and low nighttime densities (Beta to Delta). The latest model runs show a strong depletion of FeOH. See text for more details.

Langowski et al., 2015]. WACCM is a comprehensive "high top" chemistry climate model extending from the surface to 5.96×10^{-6} hPa (~140 km). The background chemistry scheme is based on that of *Kinnison et al.* [2007], which contains 59 species and 217 gas phase chemical reactions. Over 120 gas phase reactions of metallic species are then added [*Plane et al.*, 2015]. The model also includes the meteoric input function which is calculated by combining a cosmic dust astronomical model with a chemical ablation model [e.g., *Fentzke and Janches*, 2008; *Vondrak et al.*, 2008].

For this study, we compare four runs of WACCM-Fe, the Fe variant of the model [*Feng et al.*, 2013]. In contrast to the existing calculations (run Alpha), the vertical resolution in the MLT region for the new runs (Beta to Delta) was increased from around 3.5 km to less than 500 m by increasing the hybrid σ pressure vertical coordinate from 88 to 144 levels, using the same method as *Merkel et al.* [2009]. This allows for a better resolution of the highly altitude-dependent distributions of atomic H and O, which are critical for the reactions at the bottomside of the Fe layer. Run Beta uses same rate coefficients as run Alpha but the higher vertical resolution. Run Gamma increases the photolysis rate to $J(\mathrm{FeOH}) = 6 \times 10^{-3}$ s^{-1} as determined in section 3.1. Run Delta additionally changes the rate coefficients for the reaction channels of FeOH + H as described in section 3.2.

Figure 4 compares the results of the different model runs with lidar observations. We use a 24 h composite of all observations and simulations at Davis, Antarctica (69°S), for 1 month, thereby averaging out the influence of gravity waves which is apparent in Figure 1. Both WACCM-Fe and lidar data are calculated for a resolution of 30 min and integrated to 1 km. The data are smoothed with a Hann filter of 1 h and 2 km. WACCM-Fe generally simulates the high-latitude Fe layer better during winter than summer, when the model predicts an "hour glass" shape, whereas lidar observations show an uplift of the layer [*Feng et al.*, 2013; *Viehl et al.*, 2015]. Moreover, during winter the impact of ice particles potentially influencing the bottomside of the layer can be ruled out. June 2011 is the winter month with most lidar measurement (260 h).

The lidar observations in Figure 4 (solid black) show a pronounced increase of the Fe bottomside density at sunrise. During the sunlit period, densities at 76 km altitude reach around 2500 cm^{-3} and show a slight decline during the day. Densities rapidly fall after sunset and stay below 200 cm^{-3} during the dark period. Run Alpha of WACCM-Fe (dashed red) shows an increase in Fe densities during daytime, peaking toward sunset at

around 1750 cm^{-3} which significantly underestimates the observed Fe density. Also, considerable amounts of Fe persist during the dark period, which are not observed. Using the higher resolution, run Beta (dash-dotted orange) shows a more pronounced relative daytime enhancement and lower absolute densities. With the new estimate of J(FeOH), run Gamma (dash-double-dotted cyan) shows a stronger increase at sunrise. However, absolute densities are overestimated. Closer inspection of the nighttime densities shows that run Gamma predicts considerable amounts of Fe during the night, contrary to the lidar observations (see inlay in Figure 4). Run Delta (dash-triple-dotted blue) additionally uses the revised rate coefficients for reactions (1a) and (1b), which then reproduces satisfactorily the low nighttime densities. The absolute densities in run Delta peak around sunset yet are of comparable abundance to the lidar observations. Most strikingly, the timing and rate of increase at sunrise $\frac{\Delta[\mathrm{Fe}]}{\Delta t}$ in run Delta match the observed behavior very well.

A further result of this comparison is the nearly complete photolysis of FeOH during sunlit periods. Whereas run Beta shows FeOH densities of more than 3500 cm^{-3} at this altitude during all hours of the day (dark green), run Gamma calculates FeOH levels below ~300 cm^{-3} for most of the sunlit period (light green). We note that the sum of [Fe] and [FeOH] is not constant in time as Fe is further oxidized to other species.

5. Discussion and Summary

Analysis of the solar elevation dependence by *Yu et al.* [2012] demonstrated that the bottomside extension of the mesospheric Fe layer is a solar phenomenon, and FeOH is the dominant reservoir at this altitude [*Self and Plane*, 2003]. Three reactions govern this transition: the direct photolysis of FeOH and the reactions (1a) and (1b) of FeOH with atomic H. Contrary to the reactions depleting Fe, these reactions producing Fe have only been studied indirectly in the laboratory [*Self and Plane*, 2003]. Previously, the photolysis of FeOH was assumed to be negligible, with J(FeOH) set to a low value of 1×10^{-5} s^{-1} [*Plane et al.*, 2015]. Furthermore, only reaction (1a) had been considered in model simulations by *Feng et al.* [2013] with a rate coefficient of $k_{1a}=3\times10^{-10}\exp(-1264/T)$ (see section 3.2).

In the present study we have compared a new set of high-resolution WACCM-Fe model runs with different rate coefficients to our lidar observations. The crucial H and O distribution with strong gradients in the lower MLT region is thereby resolved more precisely. However, the current set of reaction rate coefficients does not reproduce the marked Fe increase at sunrise observed by lidar. A substantial increase in J (FeOH), supported by the quantum chemical calculations and consistent with lidar observations, yields a much improved simulation of the bottomside extension during sunlit hours.

However, with the previously used rate coefficient for (1a), the low nighttime densities observed by lidar in both hemispheres cannot be reproduced in the model. As section 3.2 shows, the activation energy and preexponential factor of reaction (1b) can be altered slightly to reduce the rate coefficient at mesospheric temperatures while being fast enough at high temperatures to account for Fe-catalyzed flame inhibition [*Jensen and Jones*, 1974; *Rumminger et al.*, 1999]. As a result, reaction (1a) is slower than previously assumed and reaction (1b) should not be neglected under MLT conditions. The inclusion of these new rate coefficients results in a good representation of the diurnal behavior of the Fe layer bottomside and the rate of increase at sunrise. Nevertheless, discrepancies of the model representation still persist during the afternoon hours. WACCM-Fe predicts a further increase of Fe density until sunset and a decrease later at night. This may be due to the fact that reactions (1a) and (1b) are still overestimated, although that would be difficult to reconcile with Fe combustion chemistry. Future laboratory studies would help to resolve this. Two other possibilities are that our knowledge of the neutral gas phase chemistry of Fe is incomplete, and that the diurnal variations of O and H in this altitude range are not properly captured in WACCM, which needs to be further investigated. A potential low bias of atomic O and H in WACCM would lead to even stronger constraints on reactions (1a) and (1b). Indeed, the excellent spatial and temporal resolution achievable with a modern Fe lidar provides a stringent test for a 3-D chemistry model.

We conclude that the direct photolysis of FeOH is the primary cause of the bottomside extension of the mesospheric Fe layer during sunlit hours and determine a new photolysis rate $J(\mathrm{FeOH}) = 6\times10^{-3}$ s^{-1} which is more than 2 orders of magnitude faster than previously assumed. Furthermore, contrary to previous considerations, reaction (1a) is about an order of magnitude slower and both (1a) and (1b) need to be considered under MLT conditions. These changes of rate coefficients have a profound effect on the diurnal behavior of the Fe layer at all altitudes. Tidal signatures in the Fe layer as observed by *Lübken et al.* [2011] should be strongly influenced

by this effect below the relative maximum abundance of the main reservoir FeOH at around 90 km. Improved model analyses with the new rate coefficients determined in this study will allow a deeper understanding of the dynamical and chemical properties of the MLT.

Our simulations show the strong depletion of FeOH at all altitudes whenever sunlight is present due to the increased photolysis rate. Through reaction with O3, FeOH may be oxidized to FeOOH. *Rietmeijer* [2001] has shown that α FeOOH (goethite) is a plausible candidate for MSPs. Alternatively, FeOH can dimerize efficiently [*Feng et al.*, 2013]. The nearly complete removal of FeOH as predicted by WACCM-Fe with the revised Fe chemistry therefore may have implications for an important precursor of MSP formation during sunlit periods, i.e., the whole polar summer season. Small amounts of FeOH are still present as Fe is constantly being recycled to FeOH via the reactions with O_3, O_2, H_2O, and H. Whether these amounts are sufficient to contribute to MSP formation needs to be investigated in more detail. Other metal compounds and silica might polymerize first to form embryonic particles; after which iron is added by the uptake of atomic Fe rather than Fe compounds.

We note that it may be misleading to define the bottomside of a metal layer as the 300 cm^{-3} contour [*Yu et al.*, 2012]. An analysis of $\frac{\Delta z}{\Delta t}$ shows a dependence not only on the solar elevation but also on the strongly altitude-dependent abundance of the reservoir FeOH. The slope of the bottomside extension will vary depending on whether the 300 cm^{-3} contour or any other level is defined.

In this study we have used a combination of resonance lidar observations, quantum chemical calculations, and atmospheric model simulations to determine basic physicochemical parameters (photolysis rates and rate constants) which are very challenging to measure directly. The middle atmosphere has therefore in a sense provided a natural laboratory.

Acknowledgments
The theoretical and modeling work was funded by the European Research Council (grant 291332—CODITA). The measurements at Davis were supported by the Australian Antarctic Division under Australian Antarctic science project 2325 led by R.J. Morris. T.P. Viehl and J. Höffner would like to thank their fellow expeditioners of the 64th, 65th, and 66th ANARE at Davis and the AAD staff for their dedicated support throughout the project as well as R.J. Morris and B. Kaifler for assisting with the measurements in Antarctica. We thank R. Wörl and the staff of the Andøya Space Center in Andenes, Norway, for their ongoing support with the measurements in the Arctic.

References

Chu, X, Z. Yu, C. S. Gardner, C. Chen, and W. Fong (2011), Lidar observations of neutral Fe layers and fast gravity waves in the thermosphere (110–155 km) at McMurdo (77.8°S, 166.7°E), Antarctica, *Geophys. Res. Lett.*, *38*, L23807, doi:10.1002/2011GL050016.

Delaval, J. M., C. Dufour, and J. Schamps (1980), Rotational analysis of ultraviolet systems of FeCl, *J. Phys. B: At. Mol. Phys.*, *13*, 4757–4769, doi:10.1088/022-3700/13/24/010.

Delgado, R., J. S. Friedman, J. T. Fentzke, S. Raizada, C. A. Tepley, and Q. Zhou (2012), Sporadic metal atom and ion layers and their connection to chemistry and thermal structure in the mesopause region at Arecibo, *J. Atmos. Sol. Terr. Phys.*, *74*, 11–23, doi:10.1016/j.jastp.2011.09.004.

Feng, W., D. R. Marsh, M. P. Chipperfield, D. Janches, J. Höffner, F. Yi, and J. M. C. Plane (2013), A global atmospheric model of meteoric iron, *J. Geophys. Res. Atmos.*, *118*, 9456–9474, doi:10.1002/jgrd.50708.

Feng, W., J. Höffner, D. R. Marsh, M. P. Chipperfield, E. C. M. Dawkins, T. P. Viehl, and J. M. C. Plane (2015), Diurnal variation of the potassium layer in the upper atmosphere, *Geophys. Res. Lett.*, *42*, 3619–3626, doi:10.1002/2015GL063718.

Fentzke, J. T., and C. Janches (2008), A semi-empirical model of the contribution from sporadic meteoroid sources on the meteor input function in the MLT at Arecibo, *J. Geophys. Res.*, *113*, A03304, doi:10.1029/2007JA012531.

Frankland, V. L., A. D. James, W. Feng, and J. M. C. Plane (2015), The uptake of HNO_3 on meteoric smoke analogues, *J. Atmos. Sol. Terr. Phys.*, *127*, 150–160, doi:10.1016/j.jastp.2015.01.010.

Frisch, M. J., et al. (2009), *Gaussian 09, Revision A.1*, Gaussian, Wallingford, Connecticut.

Gardner, C. S., A. Z. Liu, D. R. Marsh, W. Feng, and J. M. C. Plane (2014), Inferring the global cosmic dust influx to the Earth's atmosphere from lidar observations of the vertical flux of mesospheric Na, *J. Geophys. Res. Space Physics*, *119*, 7870–7879, doi:10.1002/2014JA020383.

Gumbel, J., and L. Megner (2009), Charged meteoric smoke as ice nuclei in the mesosphere: Part 1—A review of basic concepts, *J. Atmos. Sol. Terr. Phys.*, *71*, 1225–1235, doi:10.1016/j.jastp.2009.04.012.

Höffner, J., and J. Lautenbach (2009), Daylight measurements of mesopause temperature and vertical wind with the mobile scanning iron lidar, *Opt. Lett.*, *34*, 1351–1353.

Huang, W., X. Chu, C. S. Gardner, J. D. Carrillo-Sanchez, W. Feng, J. M. C. Plane, and D. Nesvorny (2015), Measurements of the vertical fluxes of atomic Fe and Na at the mesopause: Implications for the velocity of cosmic dust entering the atmosphere, *Geophys. Res. Lett.*, *42*, 169–175, doi:10.1002/2014GL062390.

Jensen, D. E., and G. A. Jones (1974), Catalysis of radical recombination in flames by iron, *J. Chem. Phys.*, *60*, 3412–3425, doi:10.1063/1.1681554.

Kinnison, D. E., et al. (2007), Sensitivity of chemical tracers to meteorological parameters in the MOZART-3 chemical transport model, *J. Geophys. Res.*, *112*, D20302, doi:10.1029/2006JD007879.

Langowski, M. P., C. von Savigny, J. P. Burrows, W. Feng, J. M. C. Plane, D. R. Marsh, D. Janches, M. Sinnhuber, A. C. Aikin, and P. Liebing (2015), Global investigation of the Mg atom and ion layers using SCIAMACHY/Envisat observations between 70 and 150 km altitude and WACCM-Mg model results, *J. Atmos. Sol. Terr. Phys.*, *127*, 97–102, doi:10.1016/j.jastp.2015.04.013.

Lei, J., and P. J. Dagdigian (2000), Molecular beam study of the $^6\Pi$–$X^6\Delta$ electronic transition in FeCl, *J. Chem. Phys.*, *112*, 10,221–10,227, doi:10.1063/1.481664.

Lübken, F.-J., J. Höffner, T. P. Viehl, B. Kaifler, and R. J. Morris (2011), First measurements of thermal tides in the summer mesopause region at Antarctic latitudes, *Geophys. Res. Lett.*, *38*, L24806, doi:10.1029/2011GL050045.

Lübken, F.-J., J. Höffner, T. P. Viehl, E. Becker, R. Latteck, B. Kaifler, D. Murphy, and R. J. Morris (2015), Winter/summer transition in the Antarctic mesopause region, *J. Geophys. Res. Atmos.*, *120*, 12,394–12,409, doi:10.1002/2015JD023928.

Marsh, D. R., M. J. Mills, D. E. Kinnison, J.-F. Lamarque, N. Calvo, and L. M. Polvani (2013a), Climate change from 1850 to 2005 simulated in CESM1(WACCM), *J. Clim.*, *26*, 7372–7391, doi:10.1175/JCLI-D-12-00558.1.

Marsh, D. R., D. Janches, W. Feng, and J. M. C. Plane (2013b), A global model of meteoric sodium, *J. Geophys. Res. Atmos.*, *118*, 11,442–11,452, doi:10.1002/jgrd.50870.

Megner, L., and J. Gumbel (2009), Charged meteoric smoke as ice nuclei in the mesosphere: Part 2—A feasibility study, *J. Atmos. Sol. Terr. Phys.*, *71*, 1236–1244, doi:10.1016/j.jastp.2009.05.002.

Merkel, A. W., D. R. Marsh, A. Gettelman, and E. J. Jensen (2009), On the relationship of polar mesospheric cloud ice water content, particle radius and mesospheric temperature and its use in multi-dimensional models, *Atmos. Chem. Phys.*, *9*, 8889–8901, doi:10.5194/acp-9-8889-2009.

Plane, J. M. C. (2003), Atmospheric chemistry of meteoric metals, *Chem. Rev.*, *103*(12), 4963–4984, doi:10.1021/cr0205309.

Plane, J. M. C. (2012), Cosmic dust in the Earth's atmosphere, *Chem. Soc. Rev.*, *41*, 6507–6518, doi:10.1039/c2cs35132c.

Plane, J. M. C., R. M. Cox, and R. J. Rollason (1999), Metallic metal layers in the mesopause and lower thermosphere region, *Adv. Space Res.*, *24*(11), 1559–1570.

Plane, J. M. C., W. Feng, E. M. C. Dawkins, M. P. Chipperfield, J. Höffner, D. Janches, and D. R. Marsh (2014), Resolving the strange behavior of extraterrestrial potassium in the upper atmosphere, *Geophys. Res. Lett.*, *41*, 4753–4760, doi:10.1002/2014GL060334.

Plane, J. M. C., W. Feng, and E. M. C. Dawkins (2015), The mesosphere and metals: Chemistry and changes, *Chem. Rev.*, *115*(10), 4497–4541, doi:10.1021/cr500501m.

Rietmeijer, F. J. M. (2001), Identification of Fe-rich meteoric dust, *Planet. Space Sci.*, *48*(2001), 71–77.

Rumminger, M. D., D. Reinelt, V. Babushok, and G. T. Linteris (1999), Numerical study of the inhibition of premixed and diffusion flames by iron pentacarbonyl, *Combust. Flame*, *116*(1–2), 207–219.

Saunders, R. W., S. Dhomse, W. S. Tian, M. P. Chipperfield, and J. M. C. Plane (2012), Interactions of meteoric smoke particles with sulphuric acid in the Earth's stratosphere, *Atmos. Chem. Phys.*, *12*, 4387–4398, doi:10.5194/acp-12-4378-2012.

Scalmani, G., M. J. Frisch, B. Menucci, J. Tomasi, R. Cammi, and V. Barone (2006), Geometries and properties of excited states in the gas phase and in solution: Theory and application of a time-dependent density functional theory polarizable continuum model, *J. Chem. Phys.*, *124*(9), 094107.

Schröder, D. (2008), Gaseous rust: Thermochemistry of neutral and ionic iron oxides and hydroxides in the gas phase, *J. Phys. Chem. A*, *112*, 13215–13224, doi:10.1021/jp8030804.

Self, D. E., and J. M. C. Plane (2003), A kinetic study of the reactions of iron oxides and hydroxides relevant to the chemistry of iron in the upper mesosphere, *Phys. Chem. Chem. Phys.*, *5*(7), 1407–1418, doi:10.1039/b211900e.

Tobiska, W. K., T. Woods, F. Eparvier, R. Viereck, L. Floyd, D. Bouwer, G. Rottman, and O. R. White (2000), The SOLAR2000 empirical solar irradiance model and forecast tool, *J. Atmos. Sol. Terr. Phys.*, *62*, 1233–1250.

Viehl, T. P., J. Höffner, F.-J. Lübken, J. M. C. Plane, B. Kaifler, and R. J. Morris (2015), Summer time Fe depletion in the Antarctic mesopause region, *J. Atmos. Sol. Terr. Phys.*, *127*, 97–102, doi:10.1016/j.jastp.2015.04.013.

Vondrak, T., J. M. C. Plane, S. Broadley, and D. Janches (2008), A chemical model of meteoric ablation, *Atmos. Chem. Phys.*, *8*, 7015–7031.

von Zahn, U., and J. Höffner (1996), Mesopause temperature profiling by potassium lidar, *Geophys. Res. Lett.*, *23*, 141–144.

von Zahn, U., J. Höffner, and W. J. McNeil (2002), Meteor trails as studied by ground-based lidar, in *Meteors in the Earth's Atmosphere*, edited by E. Murad and I. P. Williams, pp. 149–187, Cambridge Univ. Press, Cambridge, U. K.

Yanai, T., D. Tew, and N. Handy (2004), A new hybrid exchange-correlation functional using the Coulomb-attenuating method (CAM-B3LYP), *Chem. Phys. Lett.*, *292*, 51–57, doi:10.1016/j.cplett.2004.06.011.

Yu, Z., X. Chu, W. Huang, W. Fong, and B. R. Roberts (2012), Seasonal variations of the Fe layer in the mesosphere and lower thermosphere: Four season variability and solar effects on the layer bottomside at McMurdo (77.8°S, 166.7°E), Antarctica, *J. Geophys. Res.*, *117*, D22302, doi:10.1029/2012JD018079.